

# Detachment of a Soluble Particle at the Slag-Argon Interface: CFD Study and Experimental Observations



XIAOMENG ZHANG, SUSANNE MICHELIC, STEFAN PIRKER,  
and MAHDI SAEEDIPOUR

The behavior of non-metallic inclusions at interfaces of high-temperature melt and molten slag affects the removal of inclusions and the consequent melt cleanliness. This study presents real-time in situ observations on the behavior of an oxide particle in the vicinity of the slag-argon interface by means of high-temperature confocal scanning laser microscopy (HT-CSLM). On top of that, CFD simulations are conducted to investigate the underlying mechanisms of particle-interface interactions. In addition to revealing the particle motion process from the argon phase toward the slag, a significant particle morphology alteration associated with its dissolution in the slag is experimentally observed. Particularly, upon detachment from the slag-argon interface, the particle exhibits more dissolution at the near-interface area. By combining with numerical simulations, this study indicates that particle separation at the interface can be characterized as two stages. First, a short-term capillary force-driven motion stage happens until the particle initially settles at the interface. The settling position estimated by simulation shows good consistency with experimental measurement. Second, the particle takes a relatively long time to eventually detach from the interface, and this period is accompanied by particle dissolution. Investigations suggest that the concentration variation near the interface arising from particle dissolution triggers a Marangoni flow. This flow, in turn, enhances the local dissolution rate, consequently causing a significant particle morphology change that influences the detachment. This study provides new insight into the mechanism of inclusion removal through slag absorption in metallurgical processes. Both particle dynamics and dissolution kinetics, especially the effect of solutal Marangoni convection, are highlighted in detaching a small-scale particle from the fluid-fluid interface.

<https://doi.org/10.1007/s11663-024-03038-w>  
© The Author(s) 2024

## I. INTRODUCTION

PARTICLES interacting with fluid-fluid interfaces are widely present in nature and technological processes, from water-walking natural creatures such as water striders to flotation cleaning processes and particle-stabilized emulsions in different industries.<sup>[1–3]</sup> Many parameters related to particle characteristics, *e.g.*, particle wettability and morphology, and the nature of the

interface could affect the system's behavior.<sup>[4]</sup> Interface containing surface active species is also a rather frequent situation where the induced Marangoni flow could further alter particle dynamics.<sup>[5–7]</sup> Because of the rich theoretical foundations and practical implications, particulate interfacial systems have attracted great interest from academia and industry.

In steelmaking, non-metallic inclusions (NMIs) in the vicinity of the steel-slag interface represent such an interfacial system, which plays an important role in steel cleanliness control. As a result of steelmaking practice, NMIs inevitably exist in steel melt, for instance, as primary oxides after the addition of deoxidizers.<sup>[8]</sup> Given their detrimental effect on steel properties, they should be removed as much as possible, mainly through absorption by the molten slag covering on steel. The ability of inclusion particles to separate from the steel-slag interface and to efficiently dissolve in slag is therefore essential.<sup>[9,10]</sup> The phenomenon taking place at the interface is especially crucial for the final removal of

---

XIAOMENG ZHANG is with the K1-MET GmbH, Stahlstr. 14, Linz, 4020, Austria and also with the Department of Particulate Flow Modelling, Johannes Kepler University, Altenberger Str. 69, Linz 4040, Austria. Contact e-mail: xiaomeng.zhang@k1-met.com; SUSANNE MICHELIC is with the Chair of Ferrous Metallurgy, Montanuniversitaet Leoben, Franz Josef Str. 18, Leoben, 8700, Austria. STEFAN PIRKER and MAHDI SAEEDIPOUR are with the Department of Particulate Flow Modelling, Johannes Kepler University. Contact e-mail: mahdi.saeedipour@jku.at

Manuscript submitted September 27, 2023; accepted January 26, 2024.

Article published online March 8, 2024.

inclusions. On the one hand, particle position at the interface makes a difference in dissolution rate owing to different levels of contact with the slag, *e.g.*, fully immersed *vs* partially separated particle.<sup>[11]</sup> Moreover, the possible dissolution of entrapped particles may, in turn, affect particle separation by changing the acting forces or altering the local liquid properties.<sup>[12]</sup> Under unfavorable circumstances, inclusions trapped at the interface for a long time may adversely affect the absorption of the remaining impurities and, meanwhile, would be at risk of returning to the steel.<sup>[13,14]</sup> These interfacial events involved in the inclusion removal process remain to be investigated.

For particle interacting with a fluid-fluid interface, wettability is a decisive factor for the particle position at the interface. From the experimental point of view, the contact angle of liquid slags made with oxide substrates (representing inclusion phases) is measured using a sessile drop technique to evaluate the inclusion removal efficiency under different conditions.<sup>[15]</sup> With high-temperature confocal scanning laser microscopy (HT-CSLM), it is possible to observe particle behavior *in situ* within high-temperature steelmaking melts, such as the agglomeration of inclusions at liquid steel surfaces,<sup>[16]</sup> and even a holistic view including all processes that inclusions undergo.<sup>[17]</sup> However, it is still challenging to investigate particle separation at the interface in detail through experiments due to the short period of the motion process. Alternatively, mathematical models and numerical simulations have been developed to study particle dynamics at the interface. The mathematical model is about a force analysis for the particle in the vicinity of the steel–slag interface, taking the buoyancy, drag, and fluid added mass forces as well as the interfacial force into account.<sup>[18]</sup> Based on Newton's second law, it is possible to obtain the displacement of particle as a function of time. Three situations exist based on the particle's displacement: passing the interface, staying, and oscillating at the interface. However, the model cannot consider the interface deformation which should appear as the result of wetting. The assumption of a flat interface throughout the process leads to a less accurate estimation of the capillary force and particle motion. Recently, computational fluid dynamics (CFD) simulations have provided more insights into the interfacial separation phenomenon. Liu *et al.*<sup>[19]</sup> studied a solid particle motion at the interface with consideration of the prior drifting in steel by a phase-field model. Zhang *et al.*<sup>[20–22]</sup> simulated the particle separation process at the steel–slag interface using a dynamic mesh technique and clarified the important effects of wetting conditions and slag viscosity based on a parameter study.

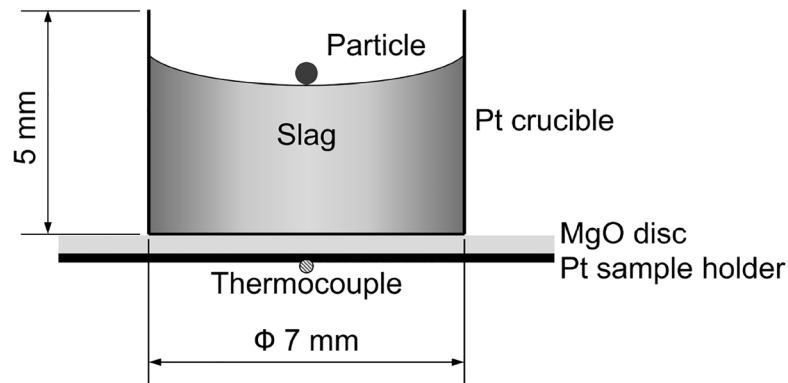
Regarding the dissolution of inclusion particles, HT-CSLM remains a powerful investigation tool.<sup>[10,23]</sup> Owing to the transparency of the slag and the well-shaped synthetic particle, the dissolution mechanism is analyzed based on the high-quality video output which shows the particle size evolution in the slag phase. In addition, it has long been known that the composition variation near the interface can lead to an interfacial tension gradient. This gradient may trigger a Marangoni

flow toward the high surface tension region. Many researchers have reported the rotation behavior of a spherical particle when conducting dissolution experiments, and they speculated that this phenomenon could be attributed to the Marangoni effect.<sup>[24]</sup> However, no follow-up studies have been conducted to examine the conjecture. There is some other evidence indicating the contribution of the Marangoni effect in metallurgical processes, for instance, local corrosions of refractories at the interfaces of gas-slag and metal-slag due to the slag film motion induced by the Marangoni effect,<sup>[25,26]</sup> surface flow of steel melt in the vicinity of the solid-melt interface because of the oxygen and sulfur segregation during solidification.<sup>[27]</sup> It indicates the importance of considering particle dissolution and the possible effect of the Marangoni flow in addition to particle dynamics while investigating particle-interface interactions.

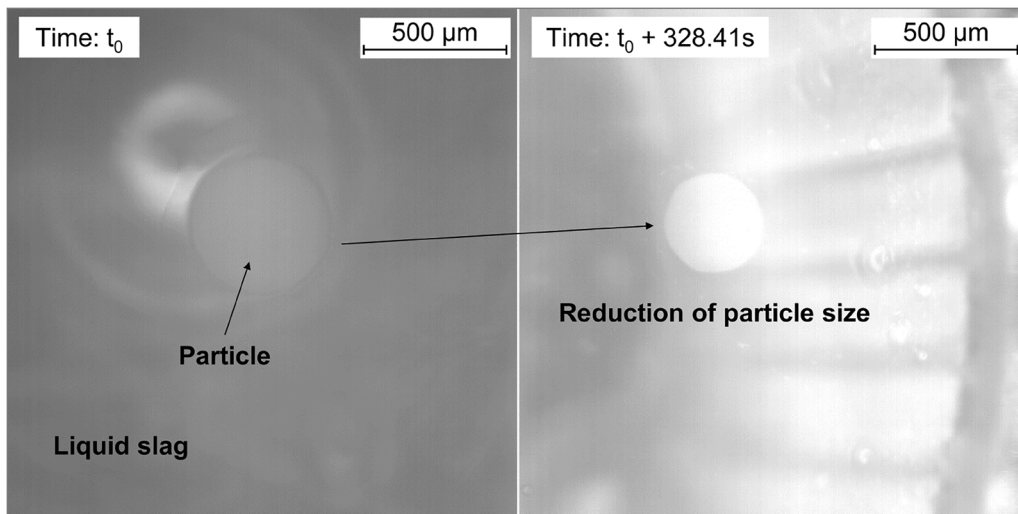
In this study, we intend to highlight a dissolution experiment conducted by HT-CSLM. Besides providing essential information on particle dissolution inside slag, this experiment constitutes a slag-argon multiphase environment and contains chemical dissolution as well as particle dynamics across the interface. Both particle movement and dissolution can be highly relevant to particle separation at the steel-slag interface. Based on experimental observations, we further use CFD simulations to explore the underlying mechanism behind the observed phenomenon, which makes follow-up investigations into particle-steel-slag systems feasible. This work aims at providing new insights into the inclusion removal process in steel production. In the meantime, it is valuable for understanding the detachment of a soluble particle at fluid-fluid interfaces in a general sense.

## II. PROBLEM DEFINITION AND HYPOTHESIS

Experimental observations presented in this study are based on the dissolution experiment performed by HT-CSLM. The general experimental setup is schematically shown in Figure 1(a). A homogeneous solidified slag chunk and a 500  $\mu\text{m}$  spherical oxide particle on top are placed inside a platinum crucible. The crucible is located on a platinum sample holder with a MgO disk in between to avoid sticking. The temperature throughout the dissolution experiment is measured with a calibrated thermocouple fixed to the bottom of the sample holder. The whole assembly is in the high-temperature chamber which is filled with high-purity argon. The current dissolution experiments are carried out at the Chair of Ferrous Metallurgy, Montanuniversitaet Leoben, Austria. The equipment used is a VL2000DX (Lasertec, Japan) type microscope combined with a SVF17SP (Yonekura, Japan) type high-temperature furnace. For more details concerning the experimental procedure, we refer to publications.<sup>[10,23]</sup> The whole experiment is recorded in video format for further analysis. Due to the good transparency of molten slag, particle profiles can be easily identified. Figure 1(b) gives an example of the extracted frames from the recorded video and the



(a)



(b)

Fig. 1—(a) Schematic representation of the setup for dissolution experiment; (b) Two instantaneous video frames showing the dissolution of inclusion.

**Table I. Investigated Slag Composition and Particle Type**

Particle Type	Slag Composition (wt pct)			
	SiO <sub>2</sub>	Al <sub>2</sub> O <sub>3</sub>	CaO	MgO
MgAl <sub>2</sub> O <sub>4</sub> Spinel	5.04	41.58	53.06	0.34

equivalent particle diameter evolution in the transparent slag. The composition of the investigated slag and the particle type are listed in Table I.

To investigate the particle dynamics while interacting with the slag-argon interface, a set of frames regarding this stage are extracted from the experimental video and shown in Figure 2. The first frame is taken before the particle starts moving and is defined as time zero. Once the slag melts, the particle quickly sinks toward the slag but still has a small area exposed to the argon highlighted in a white circle in frames (2)–(4). Over time, the exposure area becomes smaller until the particle finally detaches from the interface. What is noteworthy from the

experimental observation is that the particle rotates slightly at the moment of detachment, thus additionally showing its morphology from the side perspective, as highlighted in the last frame. It is observed that the particle is actually pear-shaped instead of retaining its original spherical shape. The outline of the particle tapering toward the top reveals that more particle dissolution happens at the region close to the slag surface.

Figure 3 displays the time-dependent changes of the particle's equivalent circular diameter (ECD) in slag and in the argon phase throughout the process consistent with Figure 2, *i.e.*, from the initial state to the final detachment. It is evident that the ECD of the particle area exposed to the argon (blue line) changes from 500  $\mu\text{m}$  to 0 as it sinks toward slag and detaches from the slag surface, and the process takes up to about 4 minutes. Moreover, the blue line confirms two stages involved in the detachment process: (1) for  $t < 20$  s, the particle moves quickly through the slag-argon interface and reaches an initial settling position at the interface (as indicated by the short plateau), and (2) over a longer period of time thereafter, particle further gradually goes



Fig. 2—A  $\text{MgAl}_2\text{O}_4$  spinel particle detaching from the slag surface observed during the experiment.

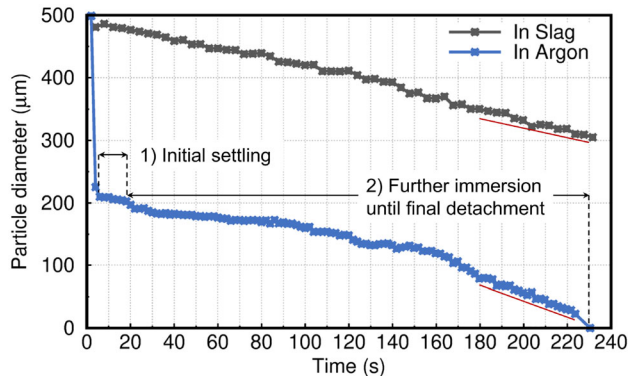


Fig. 3—Temporal variation of the equivalent circular diameter of particle in the argon (blue line) and the slag (dark gray line) phase at experimental temperature around  $1400^\circ\text{C}$  (Color figure online).

down until finally detaches from the interface. The difference in the time scale suggests that the particle behavior in the two stages might be determined by different mechanisms. In the meantime, the typical dissolution curve (represented by the dark grey line) describing the change of particle ECD in the slag shows an almost unchanged particle size in stage (1), whereas it yields an approximately linear decrease of particle size, *i.e.*, a constant particle dissolution rate in stage (2). In comparison to the typical dissolution curves, particle diameter change in argon is faster during the time close

to detachment, as indicated by the red lines, and this difference again emphasizes the significant role of the phenomena that happen near the interface.

Based on our previous work on particle dynamics at the interface,<sup>[20,21]</sup> the rapid sinking of particle toward the slag can be driven by the capillary force acting on the particle, and the particle tends to be trapped at the interface due to the combined action of capillary and viscous effects. As for the reason that leads to the eventual detachment of the particle from the interface, it could be attributed to the Marangoni effect, by which the particle shows a significant morphology change as indicated by the experiment. The detachment is expected to be closely related to the morphology change during the dissolution process. The hypothesis is further examined by conducting numerical simulations in this study, and the simulation method and results will be presented in the following sections.

### III. MODELLING AND SIMULATION

#### A. Fluid Governing Equations

To resolve the incompressible and immiscible two-phase flow, the volume of fluid (VOF) method<sup>[28]</sup> is used, where a transport equation for the volume fraction  $\alpha$  is solved together with a set of continuity and momentum equations throughout the computational domain. The governing equations read

$$\frac{\partial \rho}{\partial t} + \nabla \cdot (\rho \mathbf{U}) = 0 \quad [1]$$

$$\frac{\partial (\rho \mathbf{U})}{\partial t} + \nabla \cdot (\rho \mathbf{U} \mathbf{U}) = -\nabla p + \nabla \cdot \boldsymbol{\tau} + \rho \mathbf{g} + \mathbf{F}_\sigma + \mathbf{S}_m \quad [2]$$

$$\frac{\partial \alpha}{\partial t} + \nabla \cdot (\alpha \mathbf{U}) = 0, \quad [3]$$

where  $\mathbf{U}$  is the mixture velocity vector shared between the two phases,  $p$  is the pressure,  $\boldsymbol{\tau} = \mu(\nabla \mathbf{U} + \nabla \mathbf{U}^T)$  is the viscous stress tensor for Newtonian fluids.  $\mathbf{F}_\sigma$  denotes the volumetric representation of the surface tension force calculated by the Continuum Surface Force (CSF) approach<sup>[29]</sup> and reads

$$\mathbf{F}_\sigma = \sigma \kappa \hat{\mathbf{n}} \delta_s, \quad [4]$$

where  $\sigma$  is the surface tension coefficient, and  $\delta_s$  is a mathematical delta function approximated by  $|\nabla \alpha|$  and non-zero in interfacial cells only.  $\kappa$  is the surface curvature computed by  $\kappa = -\nabla \cdot \hat{\mathbf{n}}$  with the unit normal  $\hat{\mathbf{n}} = \nabla \alpha / |\nabla \alpha|$ . To include the effect of the contact angle that the fluid-fluid interface makes with the wall boundary, the unit normal at cells close to the particle surface is adjusted according to the three-phase contact angle  $\theta$  and is given by  $\hat{\mathbf{n}} = \hat{\mathbf{n}}_w \cos \theta + \hat{\mathbf{t}}_w \sin \theta$ , where  $\hat{\mathbf{n}}_w$  and  $\hat{\mathbf{t}}_w$  are the unit vectors normal and tangential to the wall, respectively.

The transport equation for the scalar  $\alpha$  is only solved for the secondary phase, and the value for the primary phase is computed based on the constraint that the sum of the two is up to one.  $\alpha$  further determines the phase-averaged density  $\rho = \alpha \rho_s + (1 - \alpha) \rho_a$  (subscripts  $s$  and  $a$  denote the slag and argon, respectively), and the viscosity  $\mu$  is calculated in the same way. The source term  $\mathbf{S}_m$  on the right-hand side of Eq. [2] represents the volumetric Marangoni force and will be included only when any variation in surface tension exists. In the case of concentration dependence, information on the mass fraction of species is needed to formulate  $\mathbf{S}_m$ , which is presented in the following section.

## B. Species Transport

Assuming mass transfer of dissolving species is the rate controlling step,<sup>[24,30,31]</sup> particle dissolution is simulated by solving a conservation equation for the solute mass fraction  $Y$  according to

$$\frac{\partial (\rho \alpha Y)}{\partial t} + \nabla \cdot (\rho \alpha \mathbf{U} Y) = \nabla \cdot (\rho \alpha D \nabla Y), \quad [5]$$

where  $D$  is the diffusion coefficient of solute in the slag phase. As diffusion proceeds, the surface tension will change due to variations in solute concentration, and the sensitivity depends on the parameter  $d\sigma/dY$  (that indicates the variation of surface tension with concentration). Thus, the surface tension gradient along the

interface, which induces the Marangoni flow, is calculated based on the tangential component of the concentration gradient  $\nabla_t Y = \nabla Y - \hat{\mathbf{n}}(\hat{\mathbf{n}} \cdot \nabla Y)$ . Eventually, together with the delta function  $|\nabla \alpha|$ , the volumetric Marangoni force  $\mathbf{S}_m$  is formulated as<sup>[32]</sup>

$$\mathbf{S}_m = \left[ \frac{d\sigma}{dY} (\nabla Y - \hat{\mathbf{n}}(\hat{\mathbf{n}} \cdot \nabla Y)) \right] |\nabla \alpha| \frac{2\rho}{(\rho_s + \rho_a)} \quad [6]$$

An additional density-related term is introduced to avoid high flow acceleration in the less dense fluid phase.<sup>[32]</sup> The Marangoni force  $\mathbf{S}_m$  is implemented as a user-defined function (UDF) and added to the momentum equation for the mixture phase. The simulations have been carried out using commercial software ANSYS Fluent.

## C. Simulation Setup and Particle Representation

Two modelling strategies are considered to deal with the solid spherical particle for different purposes, which are demonstrated in Figure 4 together with the general computational domain.

First, the particle is embodied by a spherical surface with the wall boundary condition, as shown in Figure 4(b), and the domain is discretized based on a dynamic overset mesh technique.<sup>[21,33]</sup> This approach enables us to simulate the motion process of particle and meanwhile to capture the capillary actions while interacting with the fluid-fluid interface. Once the fluid governing equations are solved, the resulting fluid forces and moments acting on the particle are determined by numerically integrating the pressure and the viscous components over the particle surface. Then, the movement of the particle is computed by the six degrees of freedom (6-DOF) solver based on Newton's second law. For more details, we refer to our previous study.<sup>[20,21]</sup> In that study, the particle dynamics within the water-air and steel-slag systems were investigated by combining the overset mesh and the VOF method, and excellent agreement was observed between analytics and numerical simulations. Here, the same modelling strategy is followed for particle at the slag-argon interface. Moreover, the spherical surface representation of the particle is adopted as well when particle dissolution (which essentially is a process of mass transfer from the particle surface that is saturated with dissolving species) and the solutal Marangoni effect are investigated, but the particle movement will not be taken into account during this period.

In addition, in order to show the particle morphology change during the dissolution process and the further impact of the Marangoni flow, an attempt is made to define the particle as a porous region, as displayed in Figure 4(c). The key parameter is the viscous resistance (the inverse of permeability) of the porous zone which possesses only two states. At infinite permeability, the porous region is equivalent to a fluid region; while it appears to be the solid state at zero permeability (by imposing a high viscous resistance), thus the flow cannot penetrate this region. The region's permeability depends on mass fraction and the concentration gradient of the

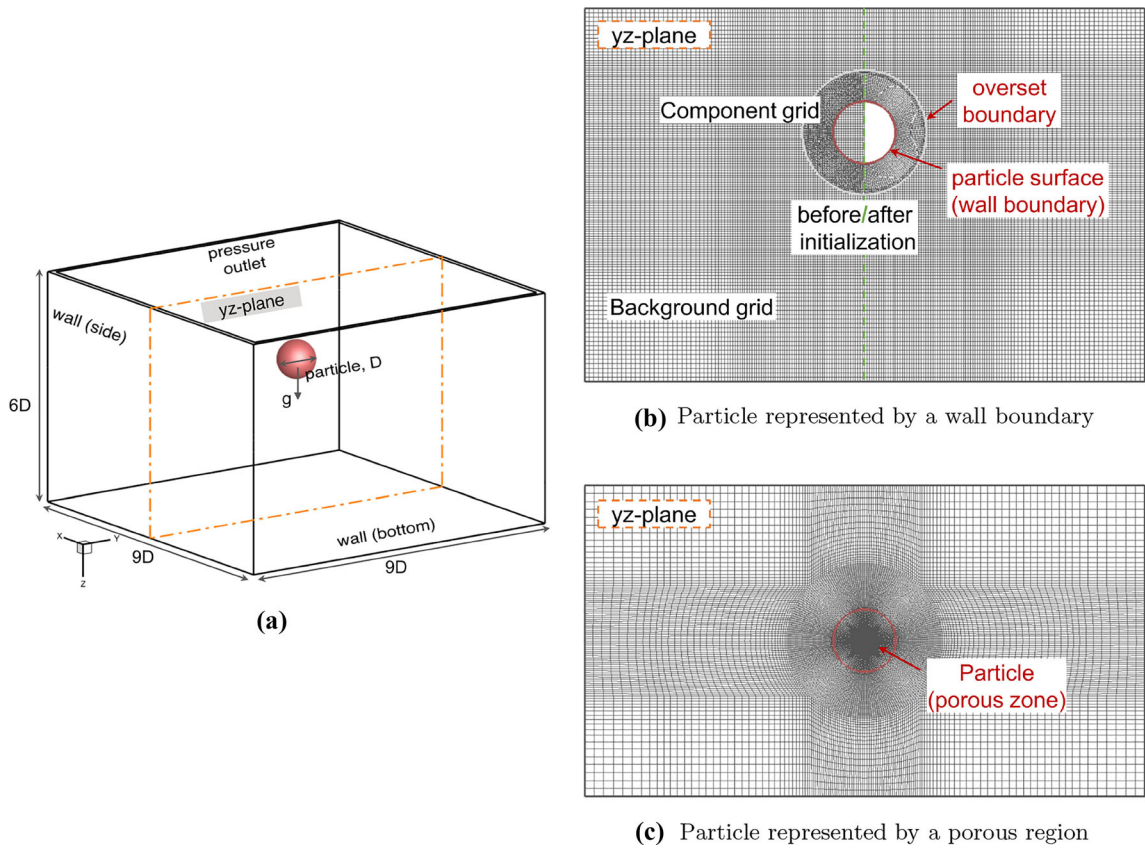


Fig. 4—(a) Computational domain and boundary conditions; (b) particle represented by a wall boundary in the frame of an overset mesh system; (c) particle considered as a porous zone using general hexahedral grid cells.

solite. Specifically, the area of saturated concentration and zero concentration gradient contains infinitesimal permeability and acts as the solid region. With this treatment, it is able to keep the core of the particle which is the undissolved part. A similar idea has been presented in Hsu's study,<sup>[34]</sup> where the shape evolution of a dissolving carbon particle was investigated. The current study is based on the porous media model in ANSYS Fluent with the implementation of a user-defined viscous resistance profile in the porous region. The flow governing equations remain the same as presented previously.

Similar to the experimental configuration, the computational domain is composed of a bottom wall, side walls, and a pressure outlet at the top. The determined domain size ( $9D \times 9D \times 9D$ ,  $D$  is the particle diameter) and mesh resolution (minimum size in  $7.62 \times 10^{-6}$  m) should be sufficient according to the sensitivity studies conducted in previous work. The simulation procedure will follow the three steps in general: (1) investigations solely on particle dynamics and its settling position are firstly conducted; (2) an additional species transport equation is solved to analyze the mass transfer process and the effect of Marangoni convection based on a fixed particle and (3) particle morphology changes during dissolution with and without the Marangoni effect are compared utilizing

the porous media model. The general properties of each phase and the parameters used for simulating different physics are given in Table II. Slag viscosity was calculated by the thermochemical software FactSage. For dissolution-related parameters,  $\Delta Y$  is the difference in mass fraction of dissolving species between the particle-slag interface and the slag bulk and represents the thermodynamic driving force for the diffusion process. For the dissolution of  $MgAl_2O_4$  spinel inclusion,  $Al_2O_3$  is chosen as the species for calculation,<sup>[35]</sup> and a small change of 0.05 (5 in mass pct) is considered in simulations. Slag surface tension  $\sigma$  approximately linearly increases with the  $Al_2O_3$  content following the relation  $\sigma = 0.3817 \times Y + 0.4155$  according to experimental studies.<sup>[36,37]</sup> All parameters are considered in a reasonable range except for the diffusion coefficient ( $D_{sim}$ ) which is larger than the value reported in the literature (in the order of  $10^{-10} \text{ m}^2 \text{ s}^{-1}$ ).<sup>[35]</sup> This is for the purpose of making the concentration field close to the three-phase contact area more visible in an affordable computational time. The fine grid resolution and very small time steps (in the order of  $10^{-6}$  s) limit the total investigation time by simulations, making it difficult to reproduce the exact experimental time scale (*i.e.*, several minutes). Nevertheless, most importantly, the order of magnitude of the Marangoni flow should not be affected if the concentration gradient is in a reasonable range.

**Table II. Overview of Physicochemical Properties for Each Phase and Parameters Used in Simulations**

General Parameters for Each Phase				
	Density $\rho$ (kg m <sup>-3</sup> )	Viscosity $\mu$ (Pa · s)	Surface Tension $\sigma_s$ (N m <sup>-1</sup> )	Size ( $\mu$ m)
Slag	2500	0.12	0.4155 <sup>[36,37]</sup>	—
Argon	1.6228	$2.125 \times 10^{-5}$	—	—
Particle	3580	—	—	500
Dissolution-Related Parameters <sup>[36,37]</sup>			Porous Region <sup>[34]</sup>	
$\Delta Y$ (wt pct)	$d\sigma/dY$ (N m <sup>-1</sup> )	$D_{\text{sim}}$ (m <sup>2</sup> s <sup>-1</sup> )	Viscous Resistance (m <sup>-2</sup> )	
5	0.3817	$2 \times 10^{-8}$	0 (fluid); $1 \times 10^{15}$ (solid)	

Slag viscosity is calculated by FactSage. Sources for other parameters can be found in the cited references.

## IV. RESULTS AND DISCUSSION

### A. Particle Motion at the Slag-Argon Interface and the Initial Settling

The results start with particle dynamics analysis. The process of a particle moving across the interface toward the slag from different perspectives obtained by simulations is shown in Figure 5. Initially, a 500  $\mu$ m spherical particle is located on the slag surface with zero velocity (Figure 5(a)), similar to the experimental scenario. Observations are first made from a front view as presented in Figure 5(b). The slag-argon interface quickly attaches the particle surface in an upcurved way ( $t = 5 \times 10^{-4}$  s). Such interface deformation can result in capillary force acting on the particle which is known as the dominant driving force for particle movement under the small-scale circumstance.<sup>[20,21]</sup> The particle continues to move downward, and it eventually gets trapped at the interface with a major part immersed in the slag ( $t = 7 \times 10^{-3}$  s). At each moment, a corresponding top view consistent with the experiment is displayed in Figure 5(c). It intuitively shows a gradual reduction of the circular diameter of the particle in the argon phase as the particle sinks into the slag. Until a certain moment ( $t = 7 \times 10^{-3}$  s), the observed circular diameter no longer changes. It should be pointed out that the ripples in diagonal directions shown in Figure 5(c) appear due to the nature of the overset mesh and should not affect the meniscus adjacent to the particle. The above observations are made based on the case of a 20 deg three-phase contact angle (on the slag side). It has to be noted that the contact angle between the investigated slag system and the inclusion phase MgAl<sub>2</sub>O<sub>4</sub> is reported in the range of 20 deg–30 deg.<sup>[15]</sup> At a larger contact angle (less wetting of slag), the particle should experience the same process but with less contact with the slag in the end compared to the case of 20 deg. Therefore, we also tested the case with a 30 deg contact angle to verify the simulation results. Figure 6 presents the temporal evolution of the circular diameter observed from the argon phase under the two different contact angles (20 deg and 30 deg), together with a comparison with the experimental measured settling position. Both curves start at 500  $\mu$ m, show a gradual decrease in the observed diameter with time, and reach a plateau at the end. In comparison,

particle shows faster movement and a better tendency to enter into slag at the smaller contact angle. In terms of the settling position, simulations provide a reliable estimate referring to the experimental value. The previous study<sup>[20]</sup> has demonstrated the combined effect of capillary action and viscous effect leading to the rapid entrapment of particle, and the details will not be repeated here. Instead, the present study aims at emphasizing the entrapment phenomenon of particle at the interface as the necessary stage of the detachment process. The particle cannot be separated from the interface if only the particle dynamics is considered.

It is essential to note that only the settling position from the experiment is taken for comparison in Figure 6, and no comparison is made about the time scale. Simulation results indicate that the particle takes only several milliseconds to settle at the interface, while the time is about 6 s for the experiment according to Figure 3. Since the video recording rate during the experiment is set to 5 fps (0.2 s interval between frames) and the data points in Figure 6 are shown in a ten-frame interval, it is therefore not possible to show experimental results on a millisecond basis. The complexity and uncertainty of experiments, such as the possible variation in fluid properties (*e.g.*, viscosity) during the slag melting process, may also contribute to some differences. Nevertheless, the key message remains the same: particle movement and settling at the interface is one of the stages in the detachment process. This stage takes an insignificant amount of time in the entire process. Thus, it is reasonable to simulate it as an independent stage and neglect any effect of dissolution in the meantime. Moreover, the experimental observations strongly indicate that further immersion and the final detachment are related to the dissolution phenomenon, and the underlying mechanisms will be discussed in the next section.

### B. Effect of the Solutal Marangoni Convection Involved in the Dissolution Process

Next to the instant settling of particle at the interface, it is the dissolution of particle inside the slag that comes into focus. The apparent particle size reduction due to dissolution, the concentration variations near the

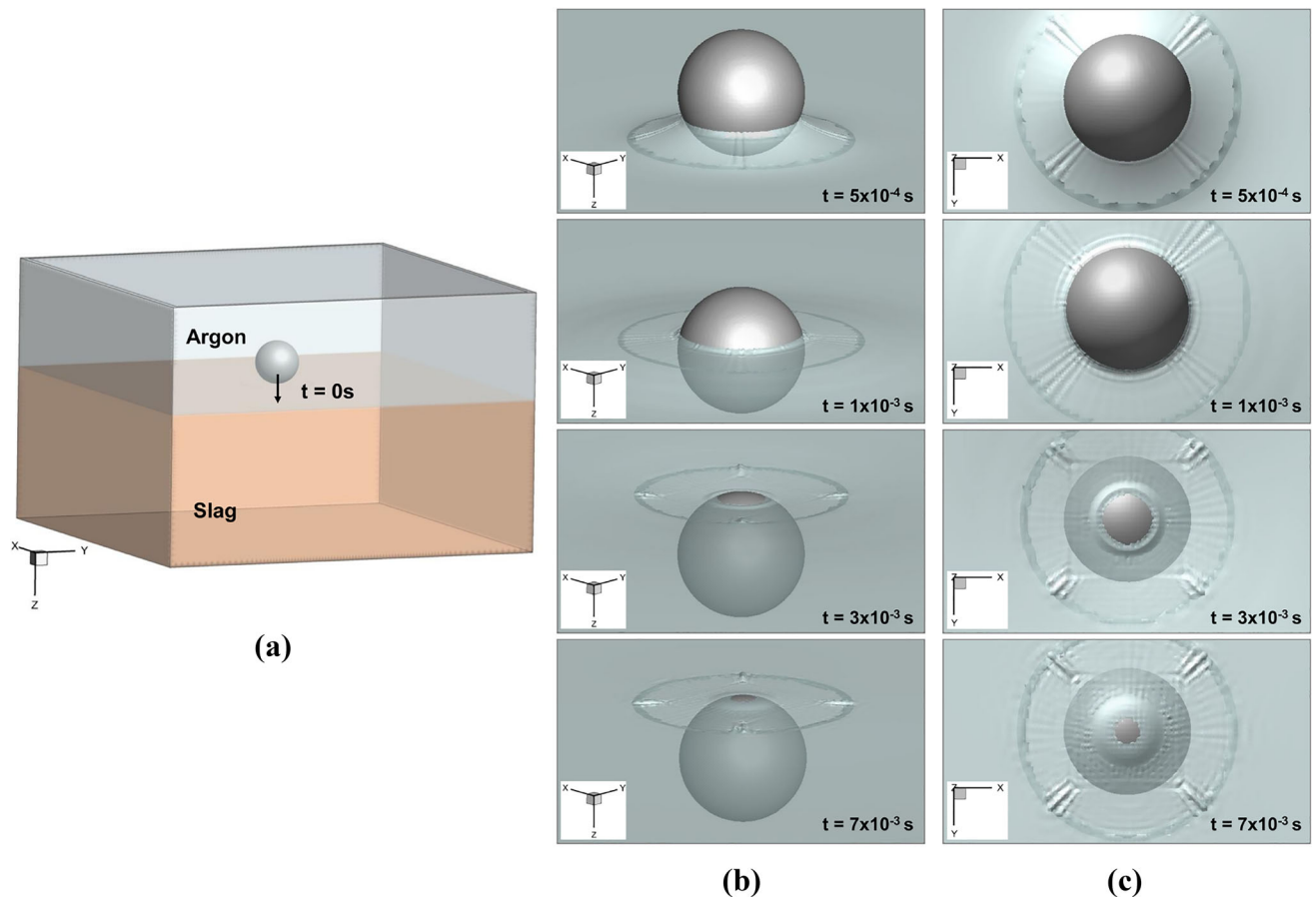


Fig. 5—Process of particle moving across the slag-argon interface. (a) The snapshot provides a full view of the initial state where a particle is located on the slag surface. Close-ups of particle motion and the evolution of the surrounding meniscus are shown in the two columns from (b) a front view and (c) a top view, respectively.

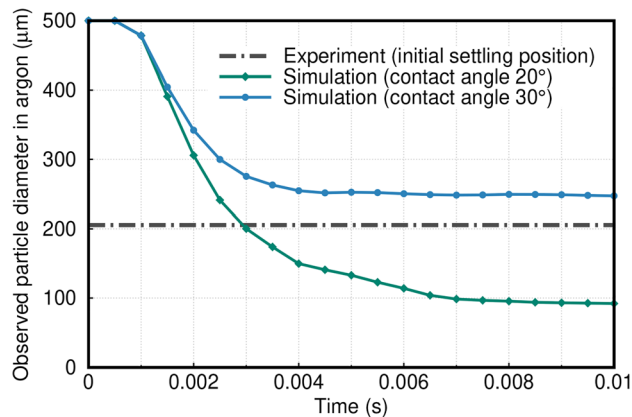


Fig. 6—Temporal evolution of the circular diameter of particle presented in argon phase.

slag-argon interface, and the possible Marangoni effect, as well as its effect on the interfacial behavior, are investigated here.

As introduced in Section III, the dissolution of  $\text{MgAl}_2\text{O}_4$  particle can be regarded as a mass transfer-controlled process, and there is no generation of intermediate reaction products. Therefore, the

dissolving species may constantly spread out to the surrounding from the particle surface which contains saturated concentration throughout the process. Consequently, a concentration gradient presents at the slag-argon interface, which results in surface tension variations due to their linear dependence. This gradient generates a Marangoni flow along the interface from areas away from the dissolving source to the near-particle sites. It is schematically illustrated in Figure 7 for the dependency of surface tension on species concentration and the corresponding Marangoni flow. For simulations, the diffusion and convection of species are simultaneously considered by solving the conservation equations, and the Marangoni effect is included by adding a source term  $\mathcal{S}_m$  (see Eq. [6]). To better understand the process, the flow characteristics are firstly analyzed in the presence and absence of the Marangoni effect, as presented in Figure 8. Figure 8(a) displays the flow field with  $|\mathcal{S}_m| = 0$ . In this situation, the noticeable velocity presents in the area close to the three-phase contact due to the capillary action. In contrast, at the same instant, with  $|\mathcal{S}_m| \neq 0$ , an inward flow toward the particle clearly appears along the slag-argon interface with a magnitude of several millimeters per second. Meanwhile, the fluid region around the particle becomes more active due to the flow that comes with the main interfacial flow,



whereas it is originally a stagnant area in the situation without the Marangoni effect. The velocity scale of the interfacial flow in the main flow direction is further compared in Figure 9(a). It can be seen that the y-component velocity is near zero at the interface when the Marangoni effect is not considered. Instead, there is an additional flow toward the particle at the same instant, and the velocity gradually decreases close to the particle surface. To estimate the effect of the interfacial flow on the flow field around the particle, we compare the velocity magnitude near the particle surface. As displayed in Figure 9(b), the value in cells adjacent to the particle surface is extracted and shown as a function of angle  $\phi$  ( $\phi$  is the central angle of the particle with a range of 0 deg to 180 deg in the counterclockwise direction). It is evident that an area ranging from  $\phi \approx 100$  deg to the three-phase contact line contains higher fluid velocity indeed when the Marangoni effect is simulated. Analyses of the flow characteristics demonstrate that the Marangoni convection can be triggered under the investigated particle-slag system. The flow velocity has a magnitude of  $O(10^{-3}) \text{ m s}^{-1}$ . It is considered reasonable in scale compared with Yin's study<sup>[27]</sup> where the Marangoni flow velocity of metal melt surface was measured using fine particles as velocity markers.

Figure 10 presents the temporal evolution of the mass fraction profiles of the dissolving species in both cases with and without the Marangoni convection. Without consideration of the Marangoni effect in simulation, it is mainly a diffusion-dominated process. In the beginning, there is a rather uniform diffusion layer around the particle. Over time, the thickness of the dissolving species layer gets wider because of further diffusion. However, due to particle entrapment at the interface, the dissolution does not take place uniformly in the radial direction. It is observed that there is a certain accumulation of dissolving species in the vicinity of the three-phase contact area (*i.e.*, the red region close to the interface in Figure 10(a), which corresponds to high solute concentration). In comparison, in the case with

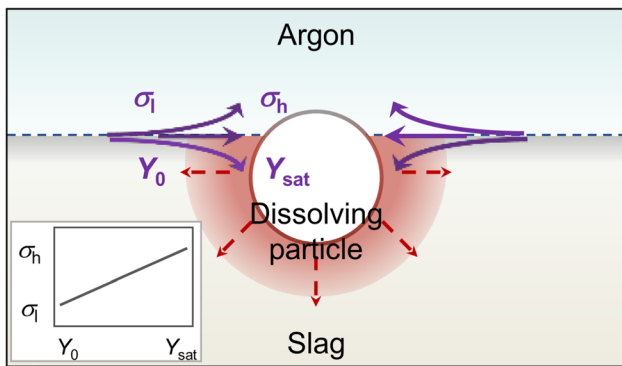


Fig. 7—Schematic illustration of the relation between slag surface tension and mass fraction of dissolving species and the induced Marangoni flow (purple arrows). As particle dissolves, a saturated concentration  $Y_{\text{sat}}$  exists around particle surface, whereas areas away from particle contain low concentration  $Y_0$ . Accordingly, slag surface tension increases toward the particle ( $\sigma_l$ : low surface tension;  $\sigma_h$ : high surface tension), and an inward flow relative to the trapped particle generates (Color figure online).

Marangoni convection involved, it is barely seen accumulated species in the same region. Besides, the thickness of the concentration layer near the equatorial plane of the particle is getting wider. Those changes are closely related to the interfacial flow and the flow near the particle surface, as depicted in Figure 8(b). Especially the flow around the particle, it is able to wash away the solute near the particle, therefore flourishing the mass transfer there. Thus, a high concentration gradient can be maintained, and the dissolution should occur faster at the corresponding region.

To compare the particle dissolution rate in the two cases, the diffusive mass flux across the particle surface (calculated by  $-\rho D \nabla Y_p$ , where  $\nabla Y_p$  is the mass fraction gradient normal to particle surface) is calculated and shown in Figure 11 as the function of angle  $\phi$ . Without the Marangoni effect, it shows a nearly constant mass flux along the major part of the particle, and the mass flux gradually decreases while approaching the interface. As diffusion proceeds, the overall mass flux at the particle surface decreases since the solute near the surface gradually tends to saturate. However, the situation becomes different when the Marangoni effect is simulated. At  $t = 0.05 \text{ s}$ , except for the part of constant mass flux similar to the former case, a much higher dissolution rate is observed at the upper part of the particle close to the interface. Over time, more areas of the particle have a higher dissolution rate. At

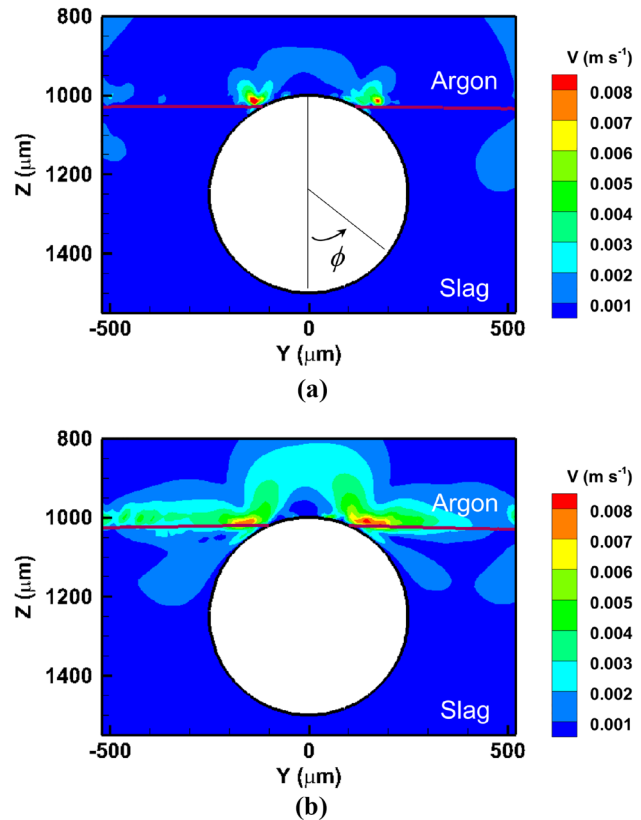


Fig. 8—Velocity contours in the vicinity of the particle and the slag-argon interface at the same instant ( $t = 0.25 \text{ s}$ ) for the case (a) without the Marangoni effect, and (b) with a source term of the Marangoni force.

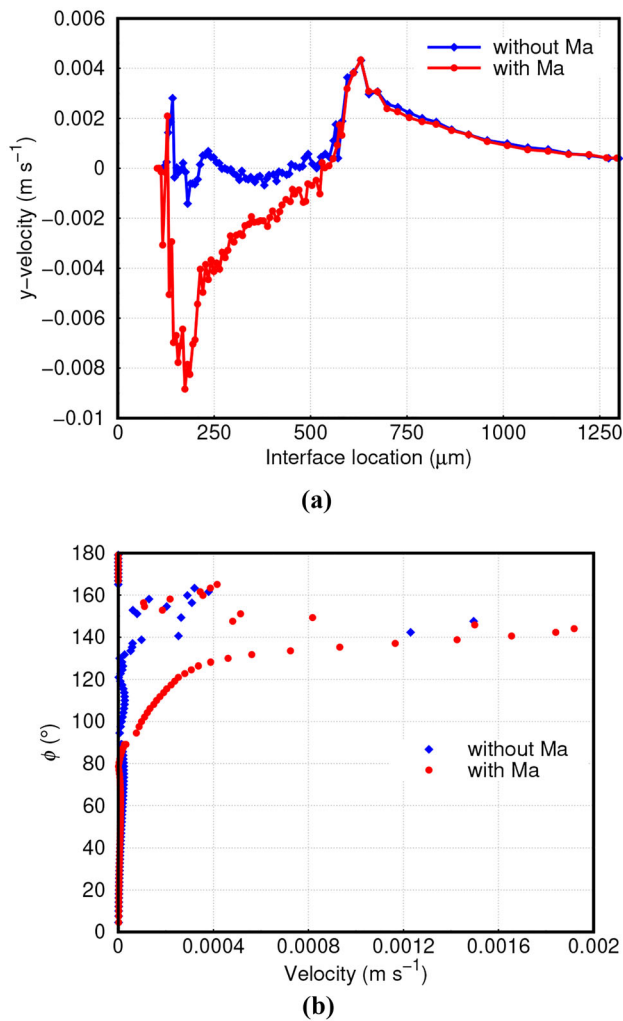


Fig. 9—(a) Fluid velocity along the interface at the main flow direction; (b) velocity magnitude near the particle surface.

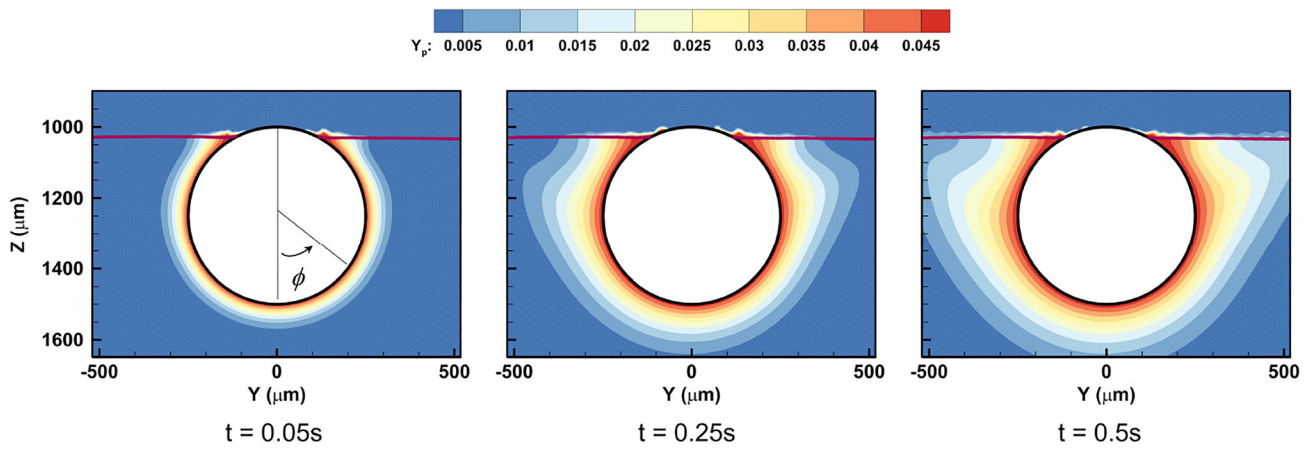
$t = 0.25$  s, it corresponds to the range of  $\phi = 100^\circ - 160^\circ$  around the particle which is consistent with the active flow region seen in Figure 8(b). A high dissolution rate is still maintained afterward. Therefore, the particle should dissolve more close to the interface in the case of Marangoni convection, which is in line with experimental observations.

In Figure 12, particle morphology evolution during the dissolution process is presented for the two cases, (a) with mainly the species diffusion dominated and (b) with the effect of the Marangoni convection based on the porous media model introduced earlier. It is observed in both cases that the particle deviates from the original spherical shape. Without considering the Marangoni effect, the shape alteration happens as a result of non-uniform dissolution due to particle entrapment at the interface. As the white line indicates, particle dissolution is slower at the region near the interface than the remaining part of the particle. This observation is consistent with the mass flux profile across the particle surface shown in Figure 11. When the Marangoni

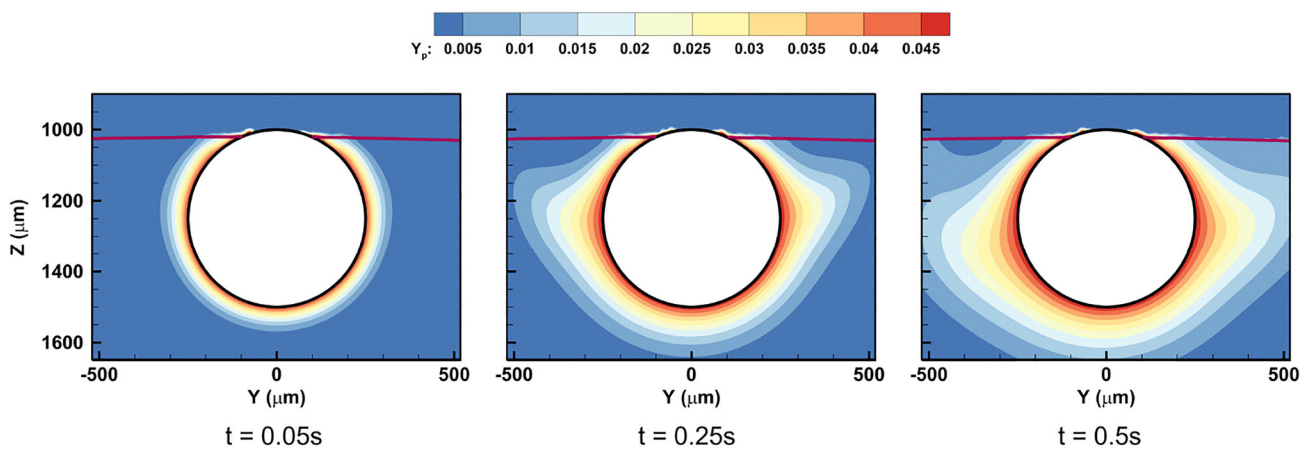
convection is taken into account, the dissolution rate in the same near-interface area increases and is even higher than the part with uniform dissolution, which is still consistent with the results from Figure 11. In this case, the particle exhibits a more noticeable morphology change and should have a more significant impact on particle movement toward detachment from the interface. However, due to the model limitations in considering the dissolution and the motion of particle simultaneously in a sufficiently long time simulation, the effect of Marangoni flow on particle separation cannot be quantified yet and remains for further study.

The above experimental observations and numerical investigations have indicated the possible contribution of the Marangoni effect in particle detachment from the slag-argon interface. The Marangoni convection presented during dissolution can enhance the local particle dissolution rate, thus changing the particle morphology significantly compared to the situation without such interfacial flow. It might be the reason for the final detachment of particle from the interface. This finding is applicable to particle removal at the steel-slag interface. Due to the high viscosity of slag, particles are mostly trapped instantly at the interface from the perspective of particle dynamics.<sup>[20]</sup> Consequently, the subsequent particle dissolution occurs in the vicinity of the steel-slag interface. With the Marangoni effect, the particle is expected to be separated and fully immersed in slag. Otherwise, the particle would be trapped at the interface for quite a long time which is comparable to the total dissolution time. Such a case could be against the absorption of the remaining inclusions, causing adverse effects on steel cleanliness. A detailed investigation into the particle-steel-slag system with the Marangoni convection will be considered in future work.

It should also be noted that the experimental observation presented in this study is not just one example occurred. But certainly, whether this is the case is related to different slag and particle combinations. Among several conducted experiments,  $\text{MgAl}_2\text{O}_4$  and  $\text{Al}_2\text{O}_3$  inclusion particles exhibit similar behavior. With the slag material presented in this study, both show the described phenomenon, *i.e.*, initial settling and final detachment with significant morphology change. For an industrial tundish slag, some convective currents and particle rotation are observed. The Marangoni effect is also believed to be involved, that makes the present finding relevant. The current study provides results in a qualitative or semi-quantitative sense due to model limitations in dealing with the multi-scale and multi-physics problem (*e.g.*, the simultaneous particle movement and particle dissolution, the large time scale for dissolution while a small-scale of the particle). Especially, it is not yet well explained regarding particle dynamics changes under the effect of morphology alteration. A more sophisticated model must be explored to study the interactions among dissolution, shape evolution and particle movement near the interface, which remains the focus of future work.



(a) without the Marangoni effect ( $|\mathbf{S}_m| = 0$ )



(b) with the Marangoni effect ( $|\mathbf{S}_m| \neq 0$ )

Fig. 10—Transient mass fraction profiles around the dissolving particle under situations (a) without the Marangoni effect and (b) with the Marangoni convection simulated.

## V. CONCLUSION

The behavior of an inclusion particle at the slag-argon interface is related to both particle dynamics and particle chemical dissolution, as indicated by experimental observations using HT-CSLM. On this basis, CFD simulations are conducted to investigate the underlying mechanisms of particle-interface interactions, especially the possible contribution of the Marangoni effect arising from species concentration variations during dissolution. Specifically, the VOF method and the overset mesh technique are used to depict the dynamic motion of the particle at the interface; a species transport equation and an additional source term in the momentum equation are included to simulate particle dissolution (mass transfer dominated process) with consideration on the effect of the Marangoni convection. The main findings can be concluded as follows:

- (1) Particle detachment at the interface can be characterized by a two-stage process. Firstly, it is a short-term capillary force-driven motion stage, and the particle ends with settling at the interface. Then, as dissolution occurs, the particle further moves toward slag until it finally detaches from the interface and is fully immersed, which takes a longer time.
- (2) The particle presents a non-spherical shape upon detachment. It is partly due to particle entrapment at the interface, which causes the non-uniform dissolution along the radial direction. Moreover, the surface tension gradient arising from concentration variations during dissolution triggers a Marangoni flow along the interface. This flow, in turn, enhances the dissolution rate locally, leading to a significant particle morphology change, as observed by a pear-shaped particle in experiments. The eventual

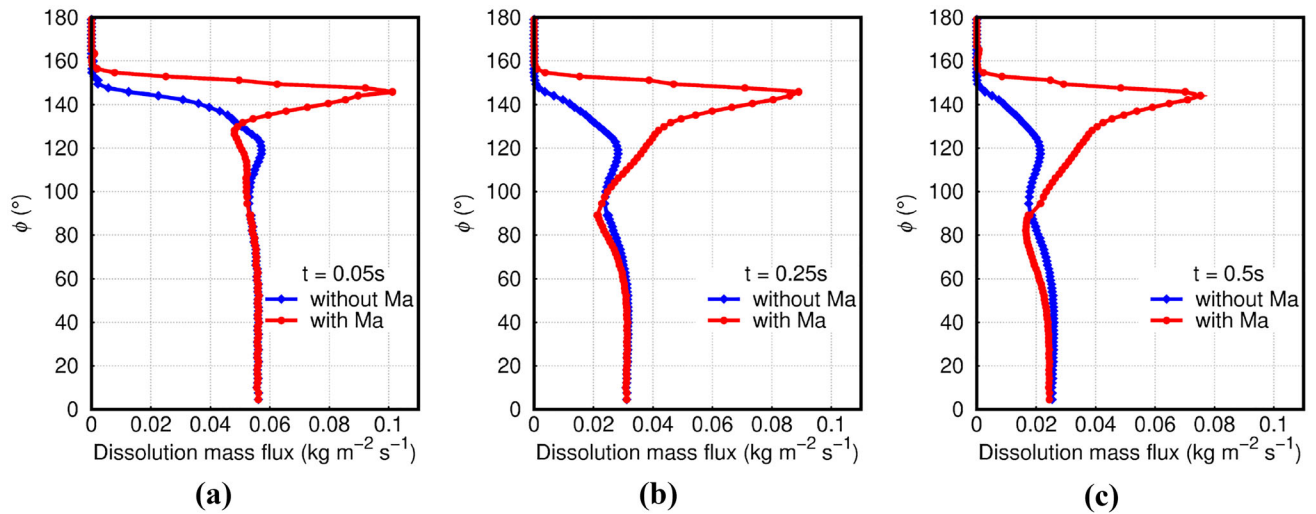


Fig. 11—Comparisons of the mass flux along the particle surface between the situation with and without the Marangoni effect involved at simulation time (a)  $t = 0.05$  s, (b)  $t = 0.25$  s and (c)  $t = 0.5$  s.

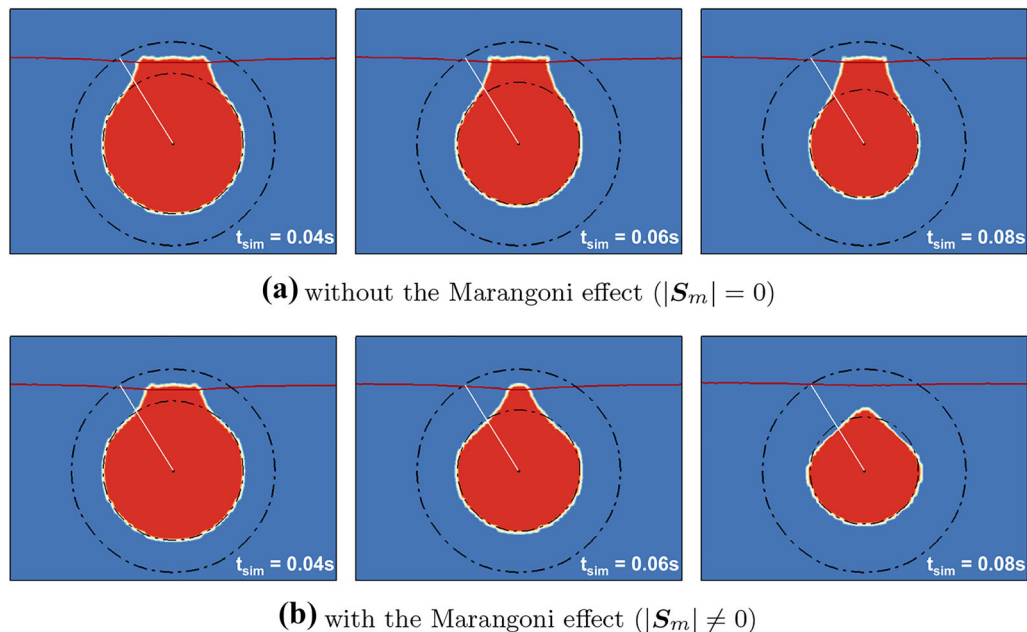


Fig. 12—Particle morphology evolution due to dissolution in slag within simulation time for the case (a) without consideration of the Marangoni effect, and (b) with the source term for the Marangoni effect. The outer dotted circle represents the initial particle size, and the inner dotted circle depicts the instant particle profile assuming a uniform dissolution in the radial direction. The red part stands for the actual particle morphology in the situations investigated. The white line connects the particle center with the initial outline to highlight the dissolution situation near the interface (Color figure online).

particle detachment can be related to its morphology change.

The presented results provide new insight into particle separation at the fluid-fluid interface with consideration of the accompanying particle dissolution. The findings can be very important for understanding the removal of non-metallic inclusions by slag absorption and steel cleanliness control. Future work will attempt to quantify the Marangoni effect on inclusion removal and look into different particle/slag combinations.

## ACKNOWLEDGMENTS

The authors gratefully acknowledge the funding support of K1-MET GmbH, metallurgical competence center. The research program of the competence center K1-MET is supported by COMET (Competence Center for Excellent Technologies), the Austrian program for competence centers. COMET is funded by the Federal Ministry for Transport, Innovation and Technology, the Federal Ministry for Science, Research and Economy, the province of Upper Austria, Tyrol

and Styria, the Styrian Business Promotion Agency. In addition to the public funding from COMET, this research project is partially financed by the industrial partners (voestalpine Stahl Linz GmbH, voestalpine Stahl Donawitz GmbH, and RHI Magnesita GmbH).

## FUNDING

Open access funding provided by Johannes Kepler University Linz.

## CONFLICT OF INTEREST

The authors declare that they have no conflict of interest.

## OPEN ACCESS

This article is licensed under a Creative Commons Attribution 4.0 International License, which permits use, sharing, adaptation, distribution and reproduction in any medium or format, as long as you give appropriate credit to the original author(s) and the source, provide a link to the Creative Commons licence, and indicate if changes were made. The images or other third party material in this article are included in the article's Creative Commons licence, unless indicated otherwise in a credit line to the material. If material is not included in the article's Creative Commons licence and your intended use is not permitted by statutory regulation or exceeds the permitted use, you will need to obtain permission directly from the copyright holder. To view a copy of this licence, visit <http://creativecommons.org/licenses/by/4.0/>.

## REFERENCES

1. J. W. Bush and D. L. Hu: *Annu. Rev. Fluid Mech.*, 38, 339–69 (2006).
2. E. Guzmán, F. Martínez-Pedrero, C. Calero, A. Maestro, F. Ortega and R. G. Rubio: *Adv. Colloid Interface Sci.*, 302, 102620 (2022).
3. A. Maestro, E. Santini, D. Zabiegaj, S. Llamas, F. Ravera, L. Liggieri, F. Ortega, R.G. Rubio, E. Guzman, et al.: *Adv. Condens. Matter Phys.*, 2015, (2015).
4. E. Guzmán, I. Abelenda-Núñez, A. Maestro, F. Ortega, A. Santamaria and R. G. Rubio: *J. Phys.: Condens. Matter*, 33, 333001 (2021).
5. S. Bekki, M. Vignes-Adler and E. Nakache: *J. Colloid Interface Sci.*, 152, 314–24 (1992).
6. G. Dunér, S. Garoff, T. M. Przybycien and R. D. Tilton: *J. Colloid Interface Sci.*, 462, 75–87 (2016).
7. W. Fei, Y. Gu and K. J. Bishop: *Curr. Opin. Colloid Interface Sci.*, 32, 57–68 (2017).
8. A. L. V. da Costa e Silva: *J. Mater. Res. Technol.*, 7, 283–99 (2018).
9. J.-Y. Choi and H.-G. Lee: *ISIJ Int.*, 43, 1348–55 (2003).
10. S. Michellic, J. Goriupp, S. Feichtinger, Y.-B. Kang, C. Bernhard and J. Schenk: *Steel Res. Int.*, 87, 57–67 (2016).
11. G. Shannon and S. Sridhar: *High Temp. Mater. Processes*, 24, 111–24 (2005).
12. A. Bozon, L. Fries, J. Kammerhofer, L. Fornoy, G. Niederreiter, S. Palzer and A. D. Salman: *Powder Technol.*, 392, 264–77 (2021).
13. S. Sridhar and A. Cramb: *Metall. Trans. B*, 31, 406–10 (2000).
14. D. Bouris and G. Bergeles: *Metall. Trans. B*, 29, 641–49 (1998).
15. B. J. Monaghan, H. Abdeyazdan, N. Dogan, M. A. Rhamdhani, R. J. Longbottom and M. W. Chapman: *ISIJ Int.*, 55, 1834–40 (2015).
16. W. Mu, N. Dogan and K. S. Coley: *JOM*, 70, 1199–209 (2018).
17. J. Cejka and S. K. Michellic: *Metals*, 13, 686 (2023).
18. K. Nakajima, K. Okamura, *Proc. 4th Int. Conf. on Molten Slags and Fluxes*, ISIJ, Sendai, p. 505 (1992).
19. W. Liu, J. Liu, H. Zhao, S. Yang and J. Li: *Metall. Trans. B*, 52, 2430–40 (2021).
20. X. Zhang, S. Pirker and M. Saeedipour: *Steel Res. Int.*, 94, 2200842 (2023).
21. X. Zhang, S. Pirker and M. Saeedipour: *Exp. Comput. Multiph. Flow*, 5, 178–91 (2023).
22. X. Zhang, S. Pirker, M. Saeedipour, In: *Proceedings of the 8th International Congress on the Science and Technology of Steel-making*, Montreal, pp. 399–408 (2022).
23. S. Feichtinger, S. K. Michellic, Y.-B. Kang and C. Bernhard: *J. Am. Ceram. Soc.*, 97, 316–25 (2014).
24. B. J. Monaghan, L. Chen and J. Sorbe: *Ironmak. Steelmak.*, 32, 258–64 (2005).
25. K. Mukai: *ISIJ Int.*, 32, 19–25 (1992).
26. G. Tsotridis: *J. Appl. Phys.*, 81, 1231–43 (1997).
27. H. Yin and T. Emi: *Metall. Trans. B*, 34, 483–93 (2003).
28. C. W. Hirt and B. D. Nichols: *J. Comput. Phys.*, 39, 201–25 (1981).
29. J. U. Brackbill, D. B. Kothe and C. Zemach: *J. Comput. Phys.*, 100, 335–54 (1992).
30. J.-Y. Choi, H.-G. Lee and J.-S. Kim: *ISIJ Int.*, 42, 852–60 (2002).
31. J. Liu, F. Verhaeghe, M. Guo, B. Blanpain and P. Wollants: *J. Am. Ceram. Soc.*, 90, 3818–24 (2007).
32. Z.S. Saldi, *Delft University of Technology*, Netherlands, Doctoral Thesis (2012).
33. Ansys® Fluent, Release 19.0, *Help system, ANSYS Fluent User's Guide Part II Section 5.5*, ANSYS, Inc, pp. 556–77 (2018).
34. S.-Y. Hsu and Y.-C. Liu: *Int. J. Heat Mass Transfer*, 127, 957–64 (2018).
35. B. J. Monaghan and L. Chen: *Ironmak. Steelmak.*, 33, 323–30 (2006).
36. K. Mukai and T. Ishikawa: *J. Japan Inst. Met. Mater.*, 45, 147–54 (1981).
37. Z. Yan, X. Lv, Z. Pang, X. Lv and C. Bai: *Metall. Trans. B*, 49, 1322–30 (2018).

**Publisher's Note** Springer Nature remains neutral with regard to jurisdictional claims in published maps and institutional affiliations.